LHCb-PHYS-2007-147
20 December 2007

# Probing the photon polarization in $\mathrm{B_s} \to \phi\gamma$ at LHCb

L. Shchutska[1,2,†], Y. Xie[3], A. Golutvin[4,1],
V. Egorychev[1], V. Shevchenko[1] and I. Belyaev[5]
[1]*ITEP, Moscow, Russia*
[2]*Moscow Institute of Physics and Technology, Russia*
[3]*University of Edinburgh, UK*
[4]*CERN, Switzerland*
[5]*Syracuse University, USA*

**Abstract**

The radiative decay $\mathrm{B_s} \to \phi\gamma$ is one of the benchmark channels in the physics programme of the LHCb experiment. It allows us to test the Standard Model through the indirect measurement of the photon polarization in $\mathrm{b} \to \mathrm{s}\gamma$ transitions. The estimation of the statistical error of the $\mathcal{CP}$-violation parameters obtained with Monte Carlo simulation is presented. It is shown that the expected statistical uncertainty in the wrong photon polarization fraction is $\sim 0.2$ with the $2\ fb^{-1}$ of integrated luminosity.

[†]E-mail: Lesya.Shchutska@cern.ch

# 1 Introduction

Measurements of inclusive radiative B meson decays $\mathrm{B} \to X_s\gamma$ [1] provide an important test for the Standard Model (SM) and set stringent bounds on physics beyond the SM [2, 3]. In addition to the rather well predicted inclusive branching ratio, which has been studied extensively both experimentally and theoretically [4, 5], there is a unique feature of this process within the SM which drew only moderate theoretical attention and which has not yet been tested: the emitted photons are left-handed in radiative $\bar{\mathrm{B}}_\mathrm{s}$ decays and are right-handed in $\mathrm{B}_\mathrm{s}$ decays. In the SM the photon in $\mathrm{b} \to \mathrm{s}\gamma$ is predominantly left-handed, owing to the $V-A$ coupling of $W$-bosons. This prediction holds in the SM up to corrections of order $m_s/m_b$ [6]. While measurements of the inclusive radiative decay rate agree with SM calculations, the helicity of photons has not yet been measured.

In several extensions of the SM the photon in $\mathrm{b} \to \mathrm{s}\gamma$ acquires an appreciable right-handed component owing to a chirality flip along a heavy fermion line in the electroweak loop process. Two well-known examples of such extensions are the left-right-symmetric model [7] and the unconstrained Minimal Supersymmetric Standard Model [8]. In both classes of models it has been demonstrated that the photons emitted in $\mathrm{b} \to \mathrm{s}\gamma$ can be largely right-handed, without affecting the SM prediction for the inclusive radiative decay rate [9]. An independent measurement of the photon helicity therefore is extremely interesting.

Several strategies have been proposed to look for signals of physics beyond the SM through helicity effects in exclusive radiative decays. In one method, the photon helicity is probed through mixing-induced $\mathcal{CP}$-asymmetries [6]. In two other schemes, angular distributions in the radiative decays of polarized $\Lambda_b$ baryons [10–12] and in $\mathrm{B} \to \mathrm{K}\pi\pi\gamma$ [13] or $\mathrm{B} \to \phi\mathrm{K}\gamma$ [14, 15] are studied.

The photon helicity effects are also accessible through the study of the time-dependent $\mathcal{CP}$-asymmetry in the $\mathrm{B}_\mathrm{s}$ system. In general, the time-dependent rate of $\mathrm{B}(\bar{\mathrm{B}})$ mesons decaying to a photon and the $\mathcal{CP}$-eigenstate $f^{CP}$ is:

$$\Gamma(\mathrm{B}_q(\bar{\mathrm{B}}_q) \to f^{CP}\gamma) \propto e^{-\Gamma_q t}\left(\cosh\frac{\Delta\Gamma_q t}{2} - \mathcal{A}^\Delta \sinh\frac{\Delta\Gamma_q t}{2} \pm \right. \\ \left. \pm \mathcal{C}\cos\Delta m_q t \mp \mathcal{S}\sin\Delta m_q t\right). \quad (1)$$

The crucial difference between the $\mathrm{B}^0$ and $\mathrm{B}_\mathrm{s}$ systems is the fact that $\Delta\Gamma_s/\Gamma_s$ is not negligible in the $\mathrm{B}_\mathrm{s}$ case and thus provides a possibility to measure $\mathcal{A}^\Delta$. Using the notation from Ref. [6, 16] it can be shown that within the SM:

$$\mathcal{S} \approx \sin 2\psi \sin\varphi,\ \mathcal{A}^\Delta \approx \sin 2\psi\cos\varphi,\ \mathcal{C} \approx 0.$$

Here $\tan\psi \equiv \left|\frac{A(\bar{\mathrm{B}}\to f^{CP}\gamma_R)}{A(\bar{\mathrm{B}}\to f^{CP}\gamma_L)}\right|$ is related to the fraction of "wrongly"-polarized photons; and $\varphi = 2\arg(V_{ts}^* V_{tb}) + \phi_R + \phi_L$ is the sum of $\mathrm{B_s}$ mixing and $\mathcal{CP}$-odd weak phases. In the SM, it is expected that $\varphi \ll 1$. The coefficient $\mathcal{S}$ is suppressed in the $\mathrm{B_s}$ system compared to the $\mathrm{B}^0$ system. However, $\cos\varphi \sim 1$ and therefore $\mathcal{A}^\Delta \approx \sin 2\psi$, a measurement of $\mathcal{A}^\Delta$ determines the "wrongly"-polarized photon fraction. Thus the study of the time-dependent rates of $\mathrm{B_s} \to \phi\gamma$ and $\bar{\mathrm{B}}_\mathrm{s} \to \phi\gamma$ allows to probe the photon helicity and therefore test the V-A structure of weak interactions in FCNC interactions.

# 2 Input parameters for the simulation

A toy Monte Carlo (MC) study was performed in order to study the statistical error of $\mathcal{S},\ \mathcal{C},\ \mathcal{A}^\Delta$. The RooFit program [17] was used for modeling probability distribution functions (PDFs) such as the reconstructed $\mathrm{B_s}$ mass and time distributions. Event distributions are defined in time and mass dimensions. Events are generated according to the appropriate PDFs and fitted with the same functional form.

## 2.1 The external input parameters

The selection study is presented in Ref. [18]. For a nominal year of LHCb data-taking ($2\ fb^{-1}$ of integrated luminosity) the signal yield is expected to be $\approx$ 11k events[1]. The background-to-signal ratio is expected to be $\frac{B}{S} < 0.95$ @ $90\%$ CL ($< 0.55$ @ $90\%$ CL after the trigger). The parameters used in the analysis are:

- $\mathrm{B_s}$ meson mass $5.367\ \mathrm{GeV}/c^2$ and lifetime $1.43\ \mathrm{ps}$ [19];
- decay rate difference between two $\mathrm{B_s}$ $\mathcal{CP}$-eigenstates $\Delta\Gamma_s = 0.084\ \mathrm{ps}^{-1}$ [19];
- $\mathrm{B_s}$ oscillation frequency $\Delta m_s = 17.77\ \mathrm{ps}^{-1}$ [20].

These values are used as input parameters for the toy MC study.

## 2.2 Signal mass distribution

In Figure 1 the reconstructed $\mathrm{B_s}$ candidate invariant mass distribution for decay $\mathrm{B_s} \to \phi\gamma$ is shown after all selection cuts are applied. The $\mathrm{B_s}$ mass resolution is given by a Gaussian distribution with central value $5.37\ \mathrm{GeV}/c^2$ and resolution $91.7 \pm 1.8\ \mathrm{MeV}/c^2$.

[1]The HLT efficiency is not considered.

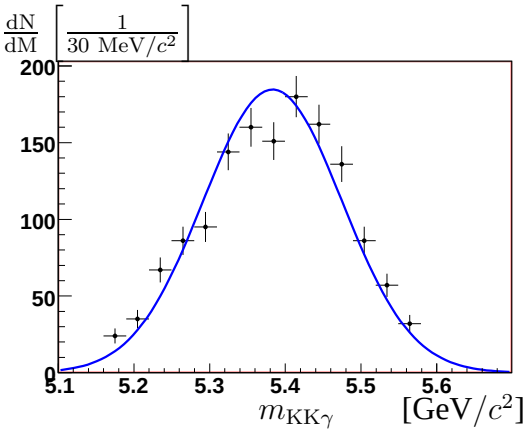


Figure 1: Signal mass distribution after the selection cuts. The curve represents the fit with the Gaussian, described in the text.

## 2.3 Background mass distribution

For background studies $\sim 4 \times 10^7$ forward $\mathrm{b\bar{b}}$-inclusive events are used. There are only five events left in the wide mass window ($\pm 1$ GeV$/c^2$) after the selection cuts [18]. In order to analyze the shape of the background, some cuts were therefore released (see Table 1). Cuts used to reject the background from primary vertices were left unchanged. The loosened selection therefore has an increased level of the combinatorial background from other B mesons decays. The obtained mass distribution is parameterized by an exponential with parameter $\mu = -0.80\ (\mathrm{GeV}/c^2)^{-1}$ (see Figure 2).

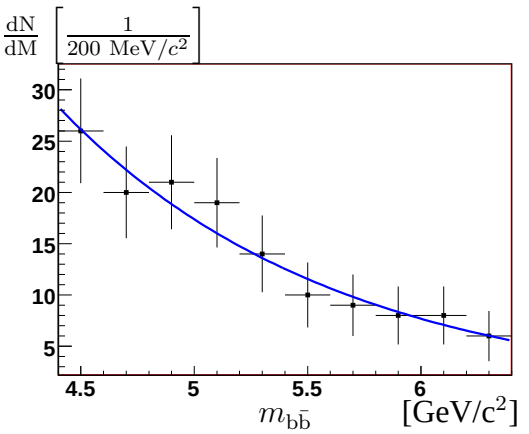


Figure 2: $\mathrm{b\bar{b}}$-inclusive background mass distribution after relaxed selection (see Table 1). The curve represents the fit with the exponential function, described in the text.

Table 1: Relaxed selection cuts:

| Measurable | Selection cut value | Relaxed cut value |
|---|---|---|
| $\mathrm{E_T^\gamma}$ | $> 2.8$ GeV | $> 2.5$ GeV |
| $\Delta \log \mathcal{L}_{\mathrm{K}\pi}$ | $> 3$ | $> 0.5$ |
| $\lvert \mathrm{M_{KK}} - 1020\ \mathrm{MeV}/c^2 \rvert$ | $< 10$ MeV/c$^2$ | $< 20$ MeV/c$^2$ |
| $\theta_{\mathrm{B}}$ | $< 10$ mrad | $< 30$ mrad |
| $\lvert \cos\theta_{\mathrm{H}} \rvert$ | $< 0.8$ | $< 1$ |

The analysis was performed in the mass interval $4.8 - 6.4\ \mathrm{GeV}/c^2$ ($\approx 17\sigma_m$) The background shape was extracted from the fit of the invariant mass distribution. The parameter of the background mass distribution $\mu$, the signal mean $\bar{m}$ and resolution $\sigma_m$ and the background-to-signal ratio $\frac{B}{S}$ are left free in the fit. The dependence of the errors on these parameters as a function of $\frac{B}{S}$ is shown in Figure 3.

## 2.4 Acceptance and the proper time resolution for signal events

The signal efficiency $\varepsilon_s(t)$ as a function of proper time was parameterized as:

$$\varepsilon_s(t) \propto \frac{(at)^c}{1 + (at)^c}. \tag{2}$$

Parameters $a$ and $c$ are found from the fit to be $a = 0.74 \pm 0.09\ \mathrm{ps}^{-1}$ and $c = 1.86 \pm 0.15$ (Figure 4). The possibility to extract the acceptance function from control channel $\mathrm{B}^0 \to \mathrm{K}^{*0}\gamma$, which is expected to have a similar acceptance function, is under study.

The proper time resolution for the signal was computed from the difference between the measured and the generated proper time distributions. It can be described as a double Gaussian with the mean value, consistent with zero ($-2 \pm 2\ fs$), resolutions of $52$ and $114\ fs$ and equal weights (see Figure 5).

The proper time resolution is dominated by the $\phi$ vertex resolution. The $\phi$ vertex is reconstructed with two kaon tracks and the error on its position increases with the decreasing of the angle $\theta$, where $\theta$ if the angle between the $\phi$ and the $\mathrm{B_s}$ flight direction in the $\mathrm{B_s}$ rest frame. Signal events are binned by the $\theta$ value and fitted with a single Gaussian. It is found that the width of this Gaussian varies from $60\ fs$ to $120\ fs$ while the angle $\theta$ changes form $\pi$ to $0$ (see Figure 7a). In Figure 6 (blue solid curves) the fit is shown for four ranges of the angle $\theta$ which are chosen in order to accumulate events with similar resolutions. The parameters of the fit are summarized in the Table 2.

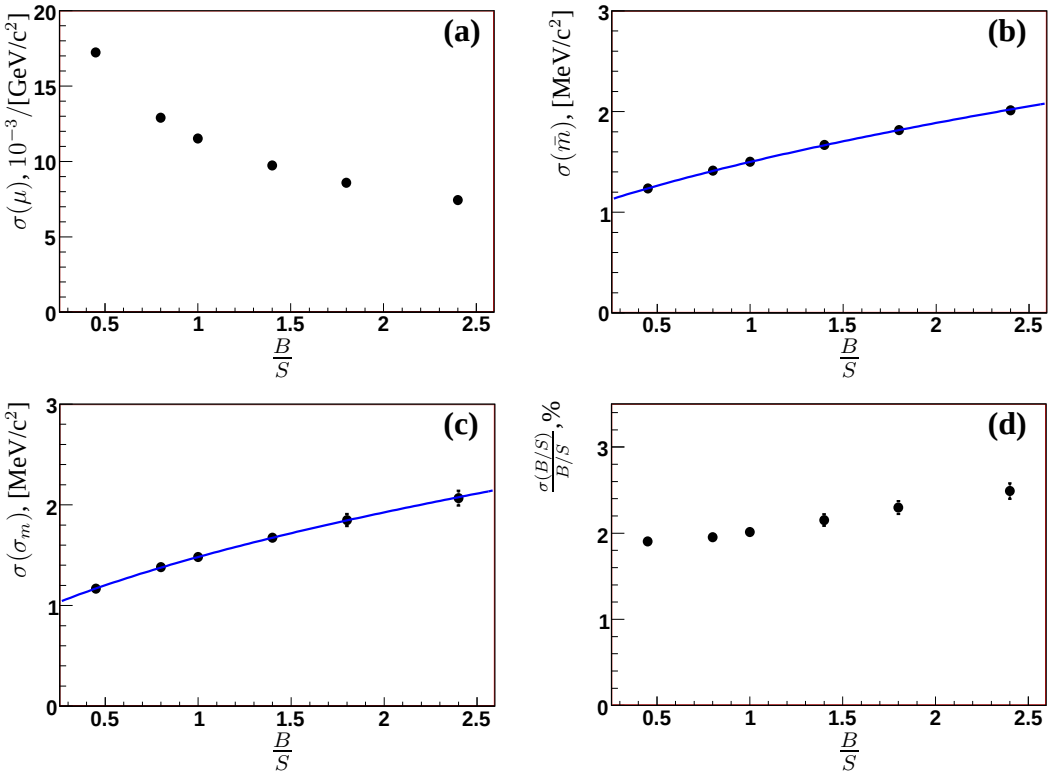


Figure 3: Errors on the parameters $\mu$, $\bar{m}$, $\sigma_m$ and $\frac{B}{S}$ obtained from the fit: a) parameter of the background exponential $\mu$; b) mean of signal Gaussian $\bar{m}$, fitted with the $f(x) \propto a_1\sqrt{1+B/S} \oplus a_2$; c) width of signal Gaussian $\sigma_m$, fitted with the $f(x) \propto a_1\sqrt{1+B/S} \oplus a_2$; d) background to signal ratio $\frac{B}{S}$.

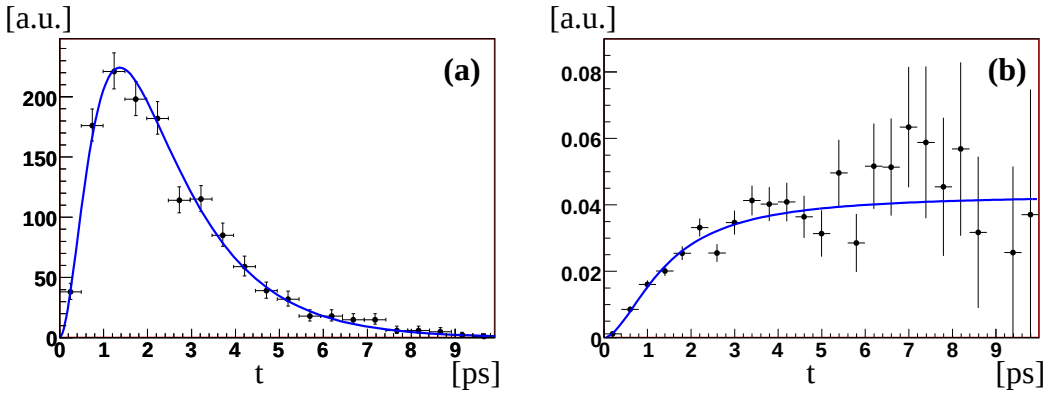


Figure 4: Signal acceptance: a) the signal MC truth proper time distribution after the selection fitted with the function $f(t) = e^{-\frac{t}{\tau}}\frac{(at)^c}{1+(at)^c}$; b) the signal acceptance as a function of proper time ([a.u.] stands for arbitrary units).

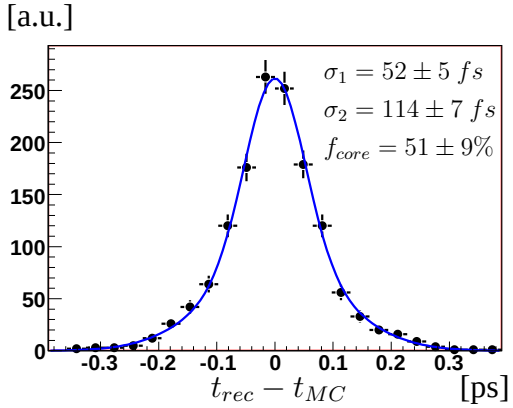


Figure 5: The proper time resolution for signal events passing the selection cuts.

The proper time resolution can also be described with the double Gaussian model with fixed widths ($\sigma_1 = 52\ fs$, $\sigma_2 = 114\ fs$) and varying component fractions (red dashed curves in Figure 6). The $f_{core}$ dependence on the angle $\theta$ is shown in Figure 7b. As expected, the fraction of core component decreases with decreasing $\theta$.

Table 2: Parameters of the signal proper time resolution obtained from the fits shown in Figure 6: the columns mean$_{1G}$ and $\sigma$ give the mean and width from the single Gaussian fit; the columns mean$_{2G}$ and $f_{core}$ give the mean and core component fraction from a fit with a double Gaussian model with fixed widths ($\sigma_1 = 52\ fs$, $\sigma_2 = 114\ fs$).

| Plot | $\cos\ \theta$ | mean$_{1G}$, $fs$ | $\sigma$, $fs$ | mean$_{2G}$, $fs$ | $f_{core}$ |
|---|---|---|---|---|---|
| a | $[-1, -0.5)$ | $10 \pm 3$ | $59 \pm 3$ | $10 \pm 3$ | $0.78 \pm 0.06$ |
| b | $[-0.5, -0.15)$ | $-8 \pm 4$ | $66 \pm 4$ | $-6 \pm 4$ | $0.66 \pm 0.06$ |
| c | $[-0.15, 0.3)$ | $-5 \pm 4$ | $88 \pm 4$ | $-4 \pm 4$ | $0.37 \pm 0.05$ |
| d | $[0.3, 1]$ | $-18 \pm 8$ | $96 \pm 7$ | $-13 \pm 8$ | $0.27 \pm 0.09$ |

A model where the proper time resolution varies with the opening angle $\alpha$ between the two kaons from the $\phi$ decay was also considered. No advantage has been found and this approach is technically more difficult and less intuitive.

In order to account for the proper time resolution, which varies with the decay angle $\theta$ the measured per-event proper time errors were considered. The pull distributions for the four ranges of the angle $\theta$ are shown in Figure 8. Their widths obtained from Gaussian fits, are represented in Table 3. Proper time errors are found to be underestimated with an average scale factor $1.35 \pm 0.03$ (Figure 9).

The distribution of proper time errors obtained from the lifetime fit to full MC

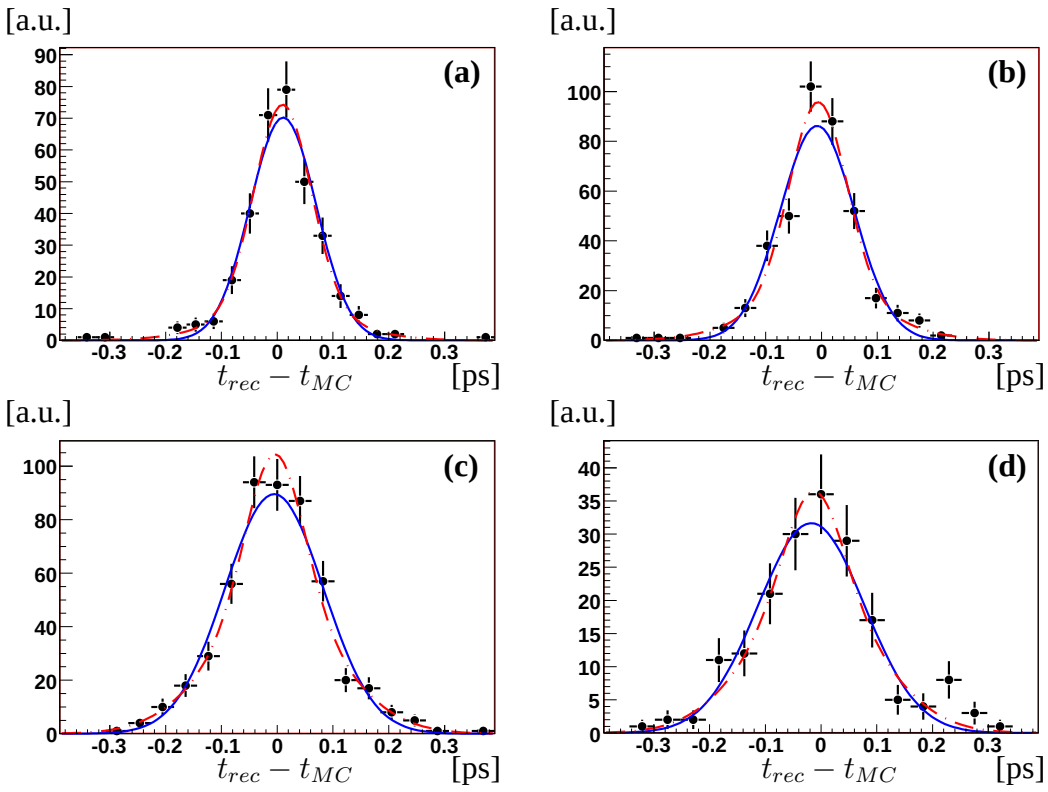


Figure 6: Proper time distribution fitted with single Gaussian (blue solid curves) and double Gaussian with $\sigma_1 = 52\ fs,\ \sigma_2 = 114\ fs$ (red dot-dashed curves) for the four ranges of decay angle $\theta$. Parameters obtained in each fit are described in Table 2.

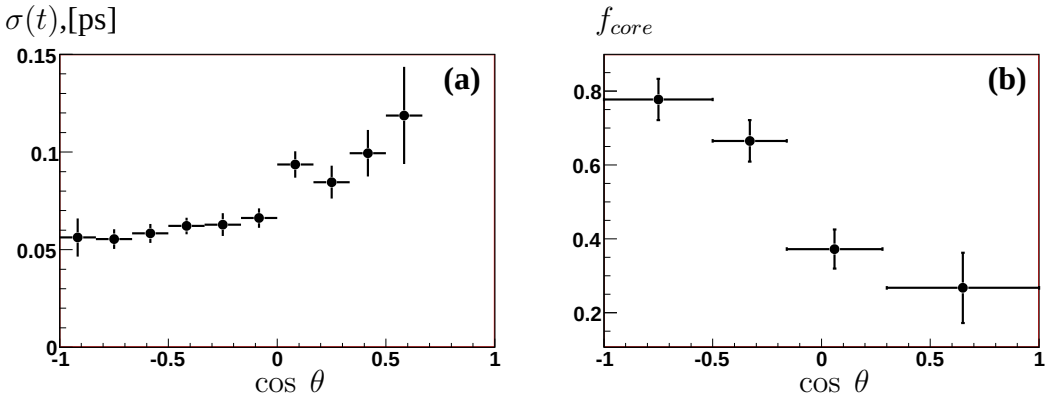


Figure 7: a) The proper time resolution as a function of the cos $\theta$; b) fraction $f_{core}$ of the narrow Gaussian as a function of the cos $\theta$.

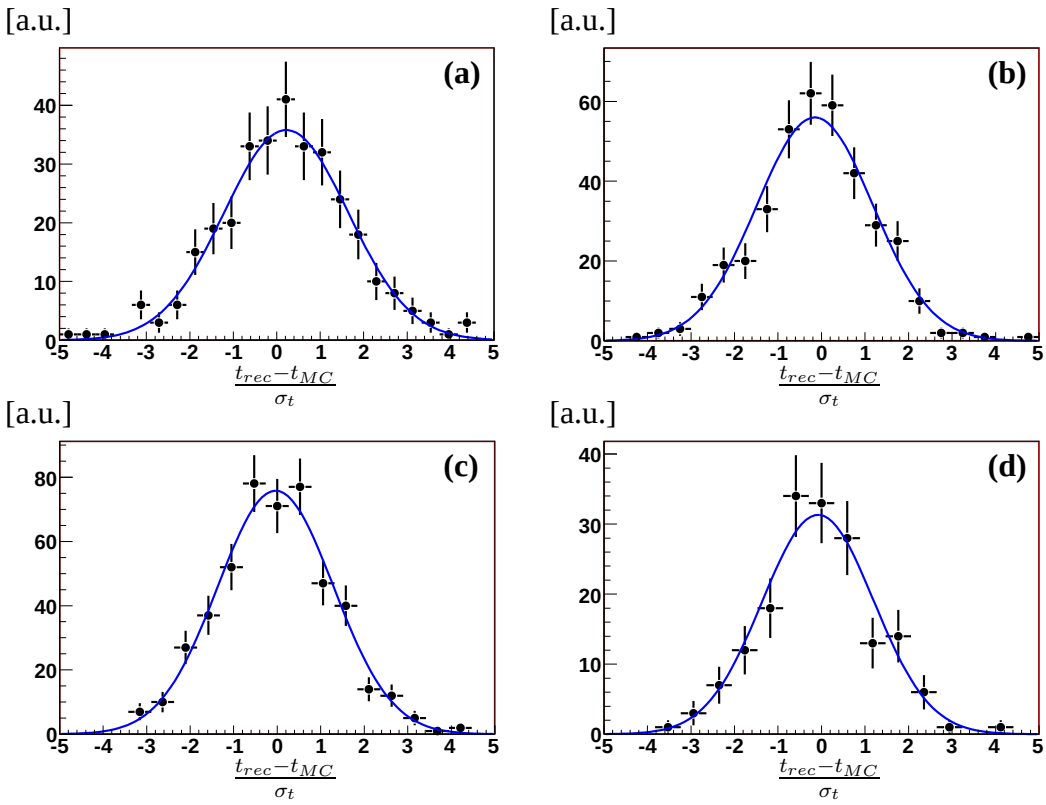


Figure 8: Proper time pull distributions for the four ranges of decay angle $\theta$ between $\phi$ and $B_s$ in $B_s$ rest system. Fit results are summarized in Table 3.

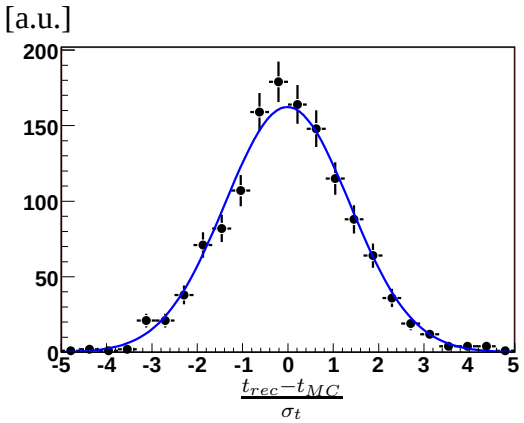


Figure 9: Proper time pull distribution for all signal events, $\sigma_{pull} = 1.35 \pm 0.03$

Table 3: Proper time pull distribution widths for four ranges of angle $\theta$ plotted on Figure 8

| Plot | $\cos\ \theta$ | mean$_{pull}$ | $\sigma_{pull}$ |
|---|---|---|---|
| a | [-1,-0.5) | $0.22 \pm 0.08$ | $1.43 \pm 0.07$ |
| b | [-0.5,-0.15) | $-0.15 \pm 0.07$ | $1.34 \pm 0.05$ |
| c | [-0.15,0.3) | $-0.04 \pm 0.06$ | $1.33 \pm 0.04$ |
| d | [0.3,1] | $-0.08 \pm 0.10$ | $1.28 \pm 0.07$ |

simulated signal events is shown in Figure 10a. The non-parametric probability density function taken from this distribution is used to generate per-event proper time errors for signal and background in toy MC studies. In Figures 10(b-d) the distribution of errors for three ranges of proper time are plotted. The errors increase slightly with the larger proper time values. This effect is neglected in the present study.

## 2.5 Distribution of background as a function of reconstructed proper time

The background proper time PDF will be determined from data from the sidebands and extrapolated to the signal region. Events obtained with the full MC simulation after relaxed selection (see Table 1) have been parameterized as:

$$\varepsilon_b(t) \propto \frac{(at)^c}{1+(at)^c}(c_1 e^{-\frac{t}{\tau_1}} + c_2 e^{-\frac{t}{\tau_2}}),$$

where the parameters values are as follows: $a$ and $c$ are fixed to $0.74\ \mathrm{ps}^{-1}$ and $1.86$, $\tau_1 = 0.45$ ps, $\tau_2 = 8.7$ ps, $c_1 = 10$ and $c_2 = 0.26$ (see Figure 11a).

Since the origin of background is found to be different in the two sidebands regions [18], it is natural that the proper time distribution is correlated with the mass. The fraction of the fast exponential component is greater in the high-mass region (see Figures 11b,12). One of the ways to introduce this correlation is to take $c_1$ and $c_2$ coefficients as linear functions of mass, in order to obtain a smooth transition between the sidebands:

$$c_1 = \alpha_0 + \alpha_1 \Delta m,\ c_2 = \beta_0 + \beta_1 \Delta m,$$

where $\Delta m = m - 5.4\ \mathrm{GeV}/c^2$. When dealing with the actual data it is possible to choose a more complicated functional form which describes the background proper time distribution in both sidebands and in the signal region.

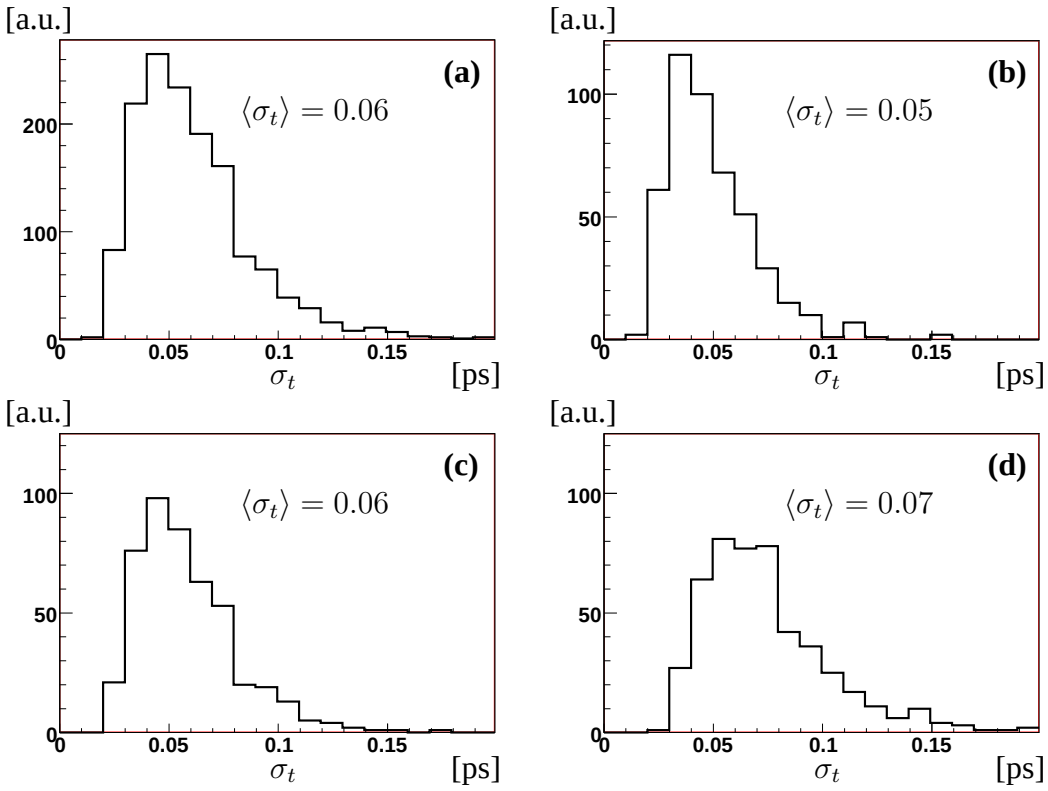


Figure 10: Proper time errors: a) all signal events passing the selection cuts; b) for events with proper time $0 < t < 1.5$ ps; c) for events with proper time $1.5 < t < 2.8$ ps; d) for events with proper time $t > 2.8$ ps.

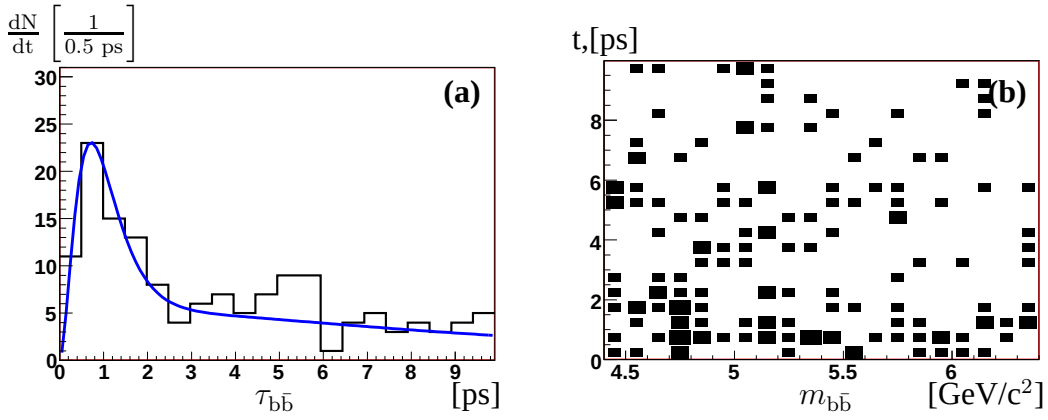


Figure 11: a) Proper time distribution of $b\bar{b}$-inclusive events after the relaxed selection (see Table 1); b) proper time vs. invariant mass distribution for $b\bar{b}$-inclusive events after the relaxed selection cuts.

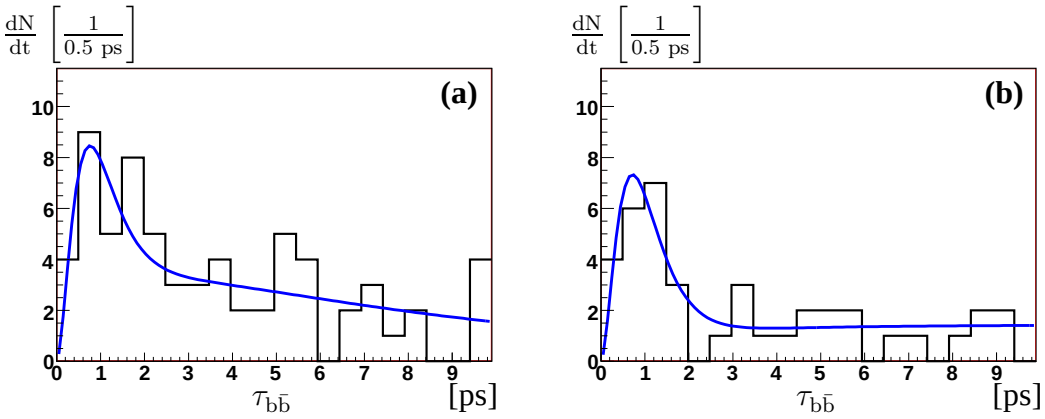


Figure 12: Proper time distribution of $b\bar{b}$-inclusive events after the relaxed selection (see Table 1): a) for left-sideband region with invariant mass 4.4-5.1 GeV$/c^2$; b) for right-sideband region with invariant mass 5.7-6.4 GeV$/c^2$.

The probability density function used for the time and mass distribution of the background is:

$$\varepsilon_b(m,t) \propto e^{-\mu m} \frac{(at)^c}{1+(at)^c} \left( (\alpha_0 + \alpha_1 \Delta m)\, e^{-\frac{t}{\tau_1}} + (\beta_0 + \beta_1 \Delta m)\, e^{-\frac{t}{\tau_2}} \right). \quad (3)$$

The simultaneous fit of background sidebands is performed with the number of background events corresponding to the set of $\frac{B}{S}$ values where the $S$ is fixed to 11k. The coefficient $\alpha_0 = 1$ is fixed. The results are summarized in Table 4. This study shows that all generated background parameters could be extracted from the data with adequate precision. The values of $\tau_1$ and $\tau_2$ are found with accuracy $3-5\%$ so they are fixed in the global fit. The other parameters are either fixed or left free in order to see whether their accuracy influences the result.

# 3 Construction of the likelihood function

In order to distinguish signal and background events, both the mass and time distributions are exploited. The following notations are introduced to simplify expressions:

$$\begin{aligned} I_+(\tau) &= \cosh \frac{\Delta\Gamma\tau}{2} - \mathcal{A}^\Delta \sinh \frac{\Delta\Gamma\tau}{2}, \\ I_-(\tau) &= \mathcal{C} \cos\, \Delta m_s \tau - \mathcal{S} \sin\, \Delta m_s \tau \end{aligned}$$

Table 4: The errors on the background shape parameters obtained from fitting the sidebands with various $B/S$ ratios. The values of input parameters are specified in the column "Input value". The parameter $\alpha_0 = 1$ is fixed.

| | | $B/S$ | | | | |
|---|---|---|---|---|---|---|
| | Input value | 0.27 | 0.55 | 0.95 | 1.5 | 2 |
| $\alpha_1$ | 0.041 | 0.22 | 0.20 | 0.17 | 0.15 | 0.13 |
| $\beta_0$ | 0.025 | 0.0017 | 0.0014 | 0.0009 | 0.0007 | 0.0006 |
| $\beta_1$ | -0.007 | 0.005 | 0.004 | 0.004 | 0.003 | 0.003 |
| $\mu$ | -0.27 | 0.27 | 0.23 | 0.20 | 0.16 | 0.14 |
| $1/\tau_1$ | 2.23 | 0.06 | 0.04 | 0.03 | 0.025 | 0.022 |
| $1/\tau_2$ | 0.118 | 0.008 | 0.005 | 0.005 | 0.004 | 0.003 |

Then probability density functions for each tagging category $\kappa$ is:

$$P_\kappa(t,m) = f_s \frac{\left\{e^{-\Gamma\tau}[I_+(\tau) + \kappa(1-2\omega)I_-(\tau)]\right\} \otimes G(t-\tau)\varepsilon(t)g_s(m)}{\int \left\{e^{-\Gamma\tau}[I_+(\tau) + \kappa(1-2\omega)I_-(\tau)]\right\} \otimes G(t'-\tau)\varepsilon(t')\mathrm{d}t'} + \\ + (1-f_s)\varepsilon_b(m,t), \quad (4)$$

where $\kappa$ can possess three values: $\kappa = -1$ corresponding to $\mathrm{B_s}$, $\kappa = 1$ to $\bar{\mathrm{B}}_\mathrm{s}$ and $\kappa = 0$ to untagged events. Here $f_s = \frac{S}{S+B}$ is the signal fraction, $\omega = 0.30$ is a wrong tagging fraction for $\mathrm{B_s}$ and $\bar{\mathrm{B}}_\mathrm{s}$ mesons [21], $G(t-\tau)$ is the proper time resolution function, $g_s(m)$ is the normalized mass PDF for signal and $\varepsilon_b(m,t)$ is the equivalent for the background as discussed in the previous sections.

The PDFs were used to construct the likelihood function:

$$\mathcal{L}_0 = \prod_{i=1}^{N_{\mathrm{B_s}}} P_{-1}(m_i,t_i,\sigma_{ti}) \prod_{i=1}^{N_{\bar{\mathrm{B}}_\mathrm{s}}} P_1(m_i,t_i,\sigma_{ti}) \prod_{i=1}^{N_{untagged}} P_0(m_i,t_i,\sigma_{ti}), \quad (5)$$

where $m_i,\ t_i,\ \sigma_{ti}$ are the measured mass, proper time and proper time error for each event, correspondingly. Here the information of the integrated decay rate is not used. Due to the fast $\mathrm{B_s}$ oscillations this information has no significant impact on the likelihood function. The number of events in each category is expected to be: $N_{\mathrm{B_s}} = N_{\bar{\mathrm{B}}_\mathrm{s}} = \frac{1}{2}\varepsilon_{tag}N_{total}$, and $N_{untagged} = (1-\varepsilon_{tag})N_{total}$. Here $\varepsilon_{tag}$ is the combined tagging efficiency for $\mathrm{B_s}$ and $\bar{\mathrm{B}}_\mathrm{s}$ mesons which is expected to be $\varepsilon_{tag} = 0.610 \pm 0.002$ [21]. As a simplification this MC study has been made assuming a single tagging category. Considering multiple tagging categories has the potential to improve the results on $\mathcal{S}$ and $\mathcal{C}$ parameters which depend on the tagging. In Ref. [21] an improvement corresponding to $24\%$ further statistics was seen by changing from a single to multiple tagging categories.

The values of $\Gamma$, $\Delta\Gamma$, $\Delta m_s$ and their experimental errors will be taken from other LHCb measurements [22, 23].

# 4 The statistical uncertainty in $CP$-asymmetry

A fast MC simulation was performed to estimate the statistical error of the measurement of the $\mathcal{S},\ \mathcal{C},\ \mathcal{A}^{\Delta}$, using as input, the signal yield, background to signal ratio, proper time acceptance functions and resolutions from the full simulation described in Section 2. This was done in the following steps :

- describe the signal and background distribution variables with a probability density function (PDF): signal mass shape as it is described in Section 2.2, signal acceptance eqn. (2), the signal proper time resolution defined with measured proper time errors from Figure 10a which was scaled by the factor 1.35 according to the pull distribution of Figure 9, background time and mass distribution eqn. (3);

- generate Monte Carlo events with 11k signal events corresponding to $2fb^{-1}$ integrated luminosity and with the background to signal ratio 0.55 in the narrow mass window 5.2-5.6 GeV/$c^2$ according to those PDFs;

- perform simultaneous fit with both tagged and untagged events with the likelihood function (5): while tagged events define the $\mathcal{S}$ and $\mathcal{C}$, untagged events give the information about $\mathcal{A}^{\Delta}$ only;

- fix the values of $\Delta\ m_s$, $\Gamma$, $\Delta\Gamma$ and also the signal acceptance, tagging efficiencies, background "lifetimes" $\tau_1,\ \tau_2$ in the fit and allow to vary the rest of the parameters;

- repeat the above steps (each called an 'experiment' ) $O(10^4)$ times.

For each experiment the fitted values of $\mathcal{S},\ \mathcal{C}$ and $\mathcal{A}^{\Delta}$ were extracted. The statistical uncertainties on the parameters $\mathcal{S},\ \mathcal{C}$ and $\mathcal{A}^{\Delta}$ were obtained from the distributions of their corresponding fitted values (see Figure 13a,b,c). The distributions were fitted with Gaussian functions. No significant biases with respect to the input values were found. The resolutions of the Gaussian fits to the distributions of fitted values were used as a measure of the statistical uncertainty in the parameters:

$$\begin{aligned} \sigma(\mathcal{A}^{\Delta}) &= 0.217 \pm 0.002 \\ \sigma(\mathcal{S}) &= 0.114 \pm 0.001 \\ \sigma(\mathcal{C}) &= 0.115 \pm 0.001 \end{aligned}$$

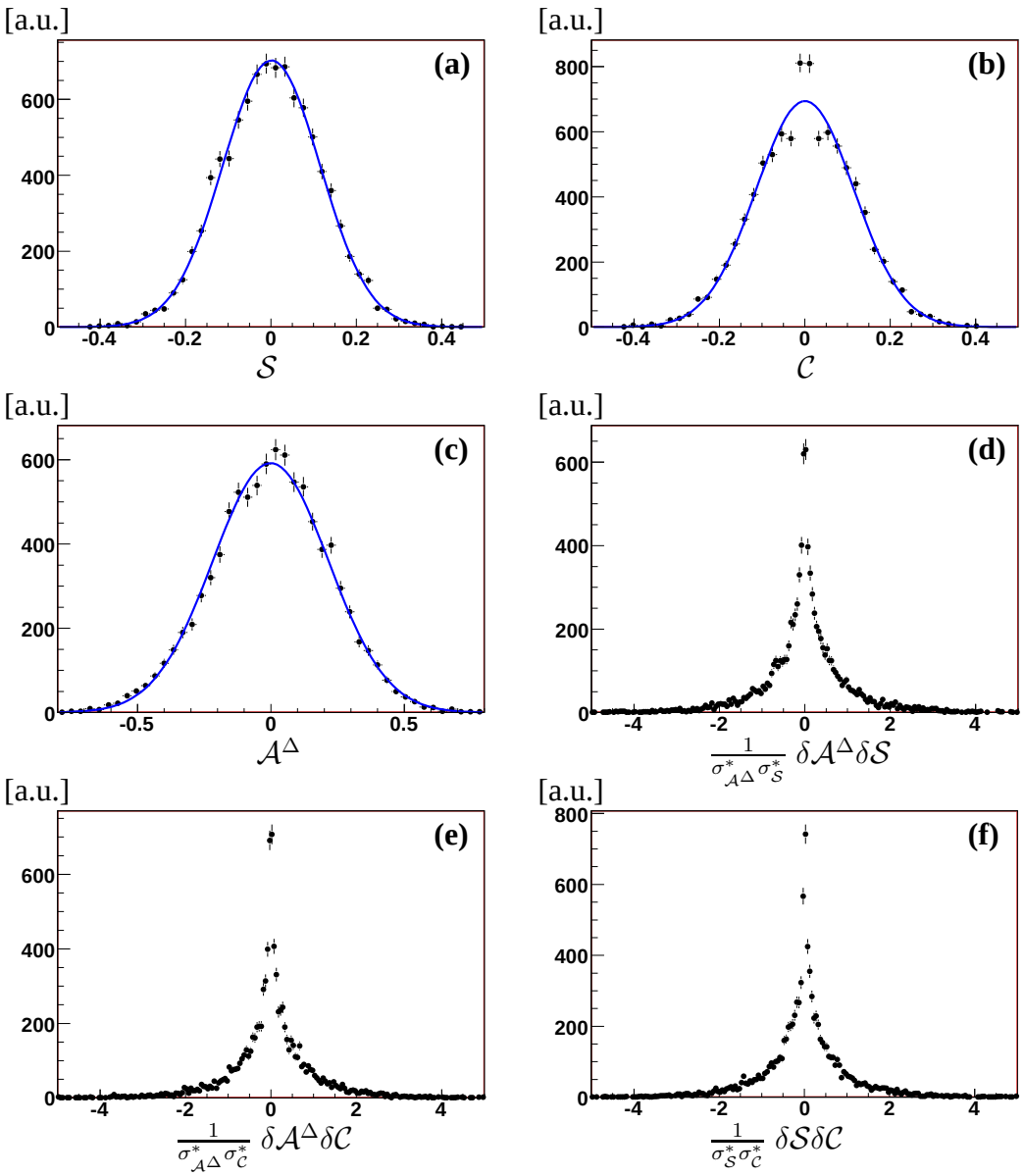


Figure 13: The distribution of fitted values of $\mathcal{S}$, $\mathcal{C}$ and $\mathcal{A}^{\Delta}$ (pictures a,b,c) from toy Monte Carlo simulations. The correlation between the $\mathcal{S}$, $\mathcal{C}$ and $\mathcal{A}^{\Delta}$ in these experiments (pictures d,e,f).

The correlation matrix is estimated to be (see Figure 13d,e,f):

$$\begin{pmatrix} 1 & 0.01 & 0.02 \\ 0.01 & 1 & 0.01 \\ 0.02 & 0.01 & 1 \end{pmatrix}.$$

The pull distributions are each essentially consistent with a Gaussian with a mean value zero and a width close to unity (see Figure 14).

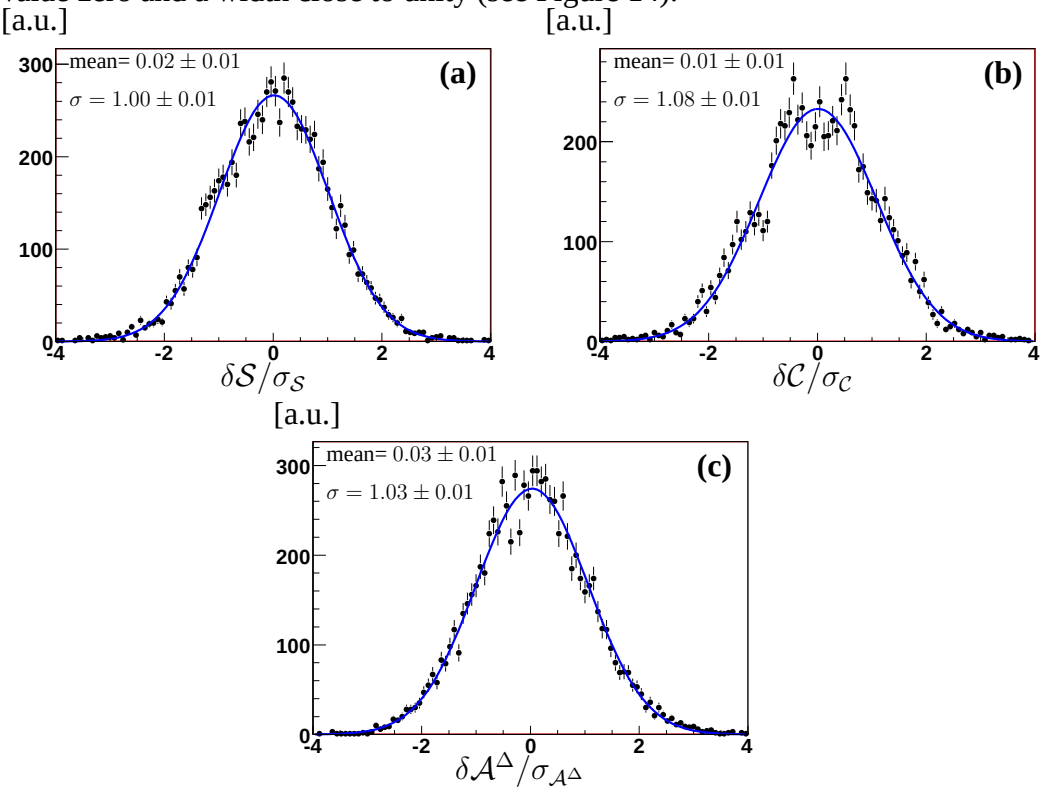


Figure 14: The pull distributions of fitted values of $\mathcal{S}$, $\mathcal{C}$ and $\mathcal{A}^{\Delta}$ from toy Monte Carlo simulations.

# 5 Stability test

The behavior of the statistical errors was explored by varying the values of external parameters one at a time.

## 5.1 Influence of the background to signal ratio

The statistical uncertainty in the $CP$-violation parameters is studied as the function of the background to signal ratio. The dependence of sensitivity is shown

in Figure 15. Red points indicate the statistical uncertainties which correspond to the upper limit at $90\%$ CL on background to signal ratio [18]. The obtained points

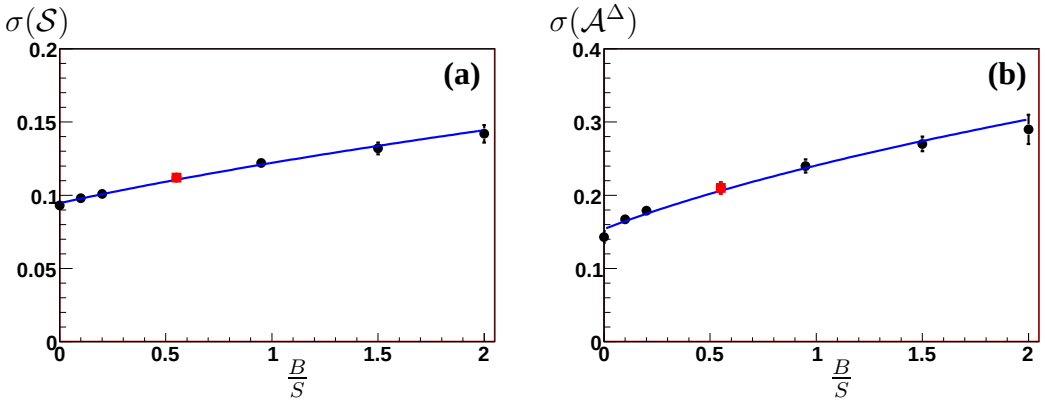


Figure 15: The estimated uncertainties in parameter $\mathcal{S}$ (a) and $\mathcal{A}^{\Delta}$ (b) as functions of the background to signal ratio in the 5.2-5.6 GeV/c$^2$ mass window

are fitted with the $f(B/S) \propto a_1\sqrt{1+B/S} \oplus a_2$ which describes the expected dependence on background level quite well.

## 5.2 Background shape

The background shape cannot be determined precisely from the available MC sample. Therefore the basic model was varied in order to understand whether it is important for the final result. The relative fraction of short- and long-lived components was first varied (see Figure 16a). The blue solid curve represents the main model used in the simulation. In the case when the relative fraction of short-lived component was doubled (green dashed curve) the obtained uncertainties are:

$$\begin{aligned} \sigma(\mathcal{A}^{\Delta}) &= 0.208 \pm 0.008 \\ \sigma(\mathcal{S}) &= 0.110 \pm 0.002. \end{aligned}$$

If this fraction is decreased twofold, the statistical errors are:

$$\begin{aligned} \sigma(\mathcal{A}^{\Delta}) &= 0.205 \pm 0.009 \\ \sigma(\mathcal{S}) &= 0.111 \pm 0.003. \end{aligned}$$

The absolute fraction of short-lived component was then increased twofold which also increases the total amount of background by 35% (see Figure 16b red dashed curve) and the uncertainties are:

$$\begin{aligned} \sigma(\mathcal{A}^{\Delta}) &= 0.220 \pm 0.009 \\ \sigma(\mathcal{S}) &= 0.116 \pm 0.003. \end{aligned}$$

When the short-lived component is decreased twofold (see Figure 16b green dashed curve) the result is:

$$\begin{aligned} \sigma(\mathcal{A}^{\Delta}) &= 0.203 \pm 0.008 \\ \sigma(\mathcal{S}) &= 0.108 \pm 0.003 \end{aligned}$$

With reasonable variations of the background shape, the statistical uncertainty

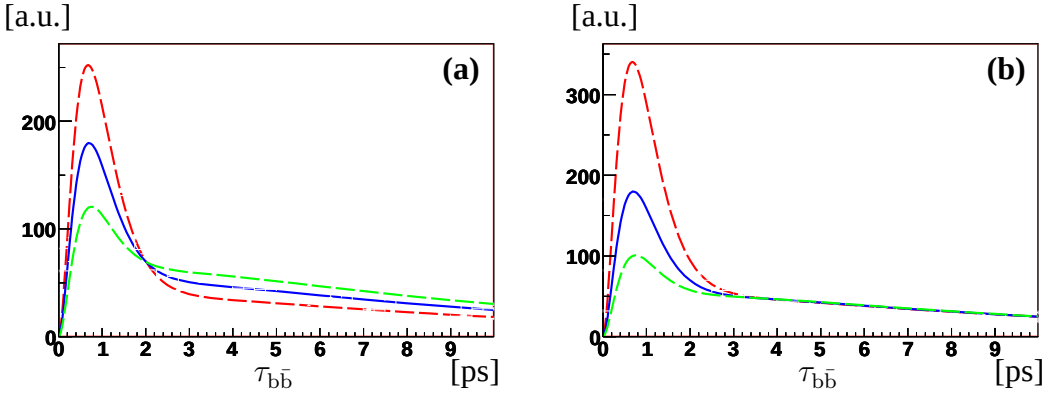


Figure 16: Proper time distribution model of $b\bar{b}$-inclusive events: blue solid curve corresponds to the main model obtained from full Monte Carlo simulation; a) red dashed upper curve represents the case when relative fraction of short-living to long-living component is doubled, green dashed lower curve shows the distribution when this fraction is decreased twofold; b) red dashed upper curve corresponds to case when absolute fraction of short-living events doubled, green dashed lower curve represents the model when this fraction is lessened twofold.

in $\mathcal{CP}$-observables stays at the same level. In case the background distribution differs somehow from the expected, the result should not worsen significantly.

## 5.3 The proper time resolution

The uncertainty in $\mathcal{S}$, $\mathcal{C}$ and $\mathcal{A}^{\Delta}$ was additionally studied as a function of the proper time resolution. Here the resolution was taken as the sum of two Gaussians with widths $52\ fs$ and $114\ fs$. When the proportion between narrow and wide resolution components is changed, the statistical uncertainty in the $\mathcal{S}$ term was found to vary from 0.30 to 0.08 (see Figure 17a), whereas the expected uncertainty in $\mathcal{A}^{\Delta}$ was not affected and stays equal to $\sim 0.21$.

The statistical uncertainty in $\mathcal{A}^{\Delta}$ depends on the $\Delta\Gamma_s/\Gamma_s$ in $B_s$ system (see Figure 17b). The obtained points are fitted with the

$$f(\Delta\Gamma_s/\Gamma_s) \propto a_1(\Delta\Gamma_s/\Gamma_s)^{-1} \oplus a_2$$

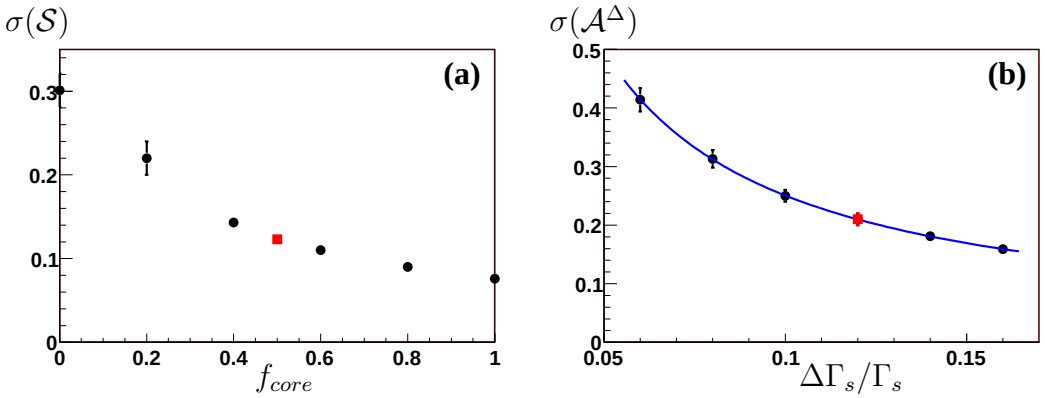


Figure 17: a) The statistical uncertainty in parameter $\mathcal{S}$ as a function of the fraction $f_{core}$ of narrow ($\sigma_1 = 52\ fs$, wide $\sigma_2 = 114\ fs$) time resolution component; b) the statistical uncertainty in $\mathcal{A}^{\Delta}$ as a function of the $\Delta\Gamma_s/\Gamma_s$.

which is consistent with the observed behavior. A value $\Delta\Gamma_s/\Gamma_s = 0.12$ was taken for this study. This is marked with square red point in the figure.

# 6 Conclusions

The fast MC simulation was performed to estimate the statistical error of the measurement of the $\mathcal{S}$, $\mathcal{C}$ and $\mathcal{A}^{\Delta}$ parameters using as input the signal yield, background-to-signal ratio, proper time acceptance functions and resolutions from the $\mathrm{B_s} \to \phi\gamma$ sample. We have estimated the uncertainties in $\mathcal{A}^{\Delta}$, $\mathcal{S}$ and $\mathcal{C}$ to be $0.22$, $0.11$ and $0.12$, correspondingly, with the signal yield 11k, $\Delta\Gamma_s/\Gamma_s = 0.12$ and using a conservative estimate for background-to-signal ratio $B/S = 0.55$ in the 5.2-5.6 GeV/$c^2$ mass window.

It has been demonstrated that the uncertainties in $\mathcal{S}$, $\mathcal{C}$ and $\mathcal{A}^{\Delta}$ have a moderate dependence on the overall background level. However the background composition does not affect the expected uncertainties significantly. The proper time resolution affects drastically the uncertainties in $\mathcal{S}$ and $\mathcal{C}$, while the uncertainty in $\mathcal{A}^{\Delta}$ has only a moderate dependence on the proper time resolution. The statistical error on $\mathcal{A}^{\Delta}$ is roughly inversely proportional to $\Delta\Gamma_s/\Gamma_s$ assuming that $\Delta\Gamma_s/\Gamma_s$ is well measured elsewhere.

# 7 Acknowledgments

We would like to express our gratitude to our colleagues from LHCb Rare decays group for the constructive comments and fruitful discussions of this work. Primarily we thank Profs. R. Forty, F. Muheim, O. Schneider and S. Stone for their attention to this work and Drs. U. Egede, P. Koppenburg, O. Leroy, C. Parkes, M. Patel and D. Martinez for the useful suggestions.

# Appendix

The theoretical decay widths for $\mathrm{B_s} \to \phi\gamma$ and $\bar{\mathrm{B}}_\mathrm{s} \to \phi\gamma$ can be conventionally parameterized as follows:

$$\Gamma_{\mathrm{B_s}\to\phi\gamma}(\tau) = |A|^2 e^{-\Gamma t}(\cosh\frac{\Delta\Gamma t}{2} - \mathcal{A}^\Delta \sinh\frac{\Delta\Gamma t}{2} + \mathcal{C}\cos\Delta m_s t - \mathcal{S}\sin\Delta m_s t)$$

$$\Gamma_{\bar{\mathrm{B}}_\mathrm{s}\to\phi\gamma}(\tau) = |A|^2 e^{-\Gamma t}(\cosh\frac{\Delta\Gamma t}{2} - \mathcal{A}^\Delta \sinh\frac{\Delta\Gamma t}{2} - \mathcal{C}\cos\Delta m_s t + \mathcal{S}\sin\Delta m_s t)$$

Observed rate for $\mathrm{B_s} \to \phi\gamma$ :

$$R(t) = \varepsilon_{tag}(\int[(1-\omega)\Gamma_{\mathrm{B_s}\to\phi\gamma}(\tau) + \omega\Gamma_{\bar{\mathrm{B}}_\mathrm{s}\to\phi\gamma}(\tau)]\varepsilon(\tau)G(\tau-t)d\tau + \frac{1}{2}B(t)) =$$

$$= \varepsilon_{tag}(\int |A|^2 e^{-\Gamma t}(\cosh\frac{\delta\Gamma t}{2} - \mathcal{A}^\Delta \sinh\frac{\delta\Gamma t}{2} +$$

$$+(1-2\omega)\mathcal{C}\cos\Delta m_s t - (1-2\omega)\mathcal{S}\sin\Delta m_s t)\varepsilon(\tau)G(\tau-t)d\tau + \frac{1}{2}B(t))$$

For $\bar{\mathrm{B}}_\mathrm{s} \to \phi\gamma$ :

$$\bar{R}(t) = \varepsilon_{tag}(\int[\omega\Gamma_{\mathrm{B_s}\to\phi\gamma}(\tau) + (1-\omega)\Gamma_{\bar{\mathrm{B}}_\mathrm{s}\to\phi\gamma}(\tau)]\varepsilon(\tau)G(\tau-t)d\tau + \frac{1}{2}B(t)) =$$

$$= \varepsilon_{tag}(\int |A|^2 e^{-\Gamma t}(\cosh\frac{\delta\Gamma t}{2} - \mathcal{A}^\Delta \sinh\frac{\delta\Gamma t}{2} -$$

$$-(1-2\omega)\mathcal{C}\cos\Delta m_s t + (1-2\omega)\mathcal{S}\sin\Delta m_s t))\varepsilon(\tau)G(\tau-t)d\tau + \frac{1}{2}B(t))$$

Untagged rate:

$$R_{untagged}(t) = (1-\varepsilon_{tag})(\int[\Gamma_{\mathrm{B_s}\to\phi\gamma}(\tau) + \Gamma_{\bar{\mathrm{B}}_\mathrm{s}\to\phi\gamma}(\tau)]\varepsilon(\tau)G(\tau-t)d\tau + B(t)) =$$

$$= (1-\varepsilon_{tag})(\int |A|^2 e^{-\Gamma t}(\cosh\frac{\delta\Gamma t}{2} - \mathcal{A}^\Delta \sinh\frac{\delta\Gamma t}{2})\varepsilon(\tau)G(\tau-t)d\tau + B(t))$$

# References


[1] M. S. Alam *et al.* [CLEO Collaboration], Phys. Rev. Lett. **74** (1995) 2885; S. Chen *et al.* [CLEO Collaboration], Phys. Rev. Lett. **87** (2001) 251807 [arXiv:hep-ex/0108032]; R. Barate *et al.* [ALEPH Collaboration], Phys. Lett. B **429** (1998) 169; K. Abe *et al.* [Belle Collaboration], Phys. Lett. B **511** (2001) 151 [arXiv:hep-ex/0103042].

[2] T. Hurth, Frascati Phys. Ser. **41** (2006) 325.

[3] See e.g. P. Gambino, J. Phys. G **27**, 1199 (2001), and references therein.

[4] See e.g. A. Ali and A. Parkhomenko, arXiv:hep-ph/0610149, and references therein.

[5] M. Misiak, arXiv:hep-ph/0105312, proceedings of the XXXVIth Rencontres de Moriond, Les Arcs, March 10-17, 2001, and references therein.

[6] D. Atwood, M. Gronau and A. Soni, Phys. Rev. Lett. **79** (1997) 185 [arXiv:hep-ph/9704272].

[7] R. N. Mohapatra and J. C. Pati, Phys. Rev. D **11** (1975) 566; G. Senjanovic and R. N. Mohapatra, Phys. Rev. D **12** (1975) 1502; G. Senjanovic, Nucl. Phys. B **153** (1979) 334.

[8] H. E. Haber and G. L. Kane, Phys. Rept. **117** (1985) 75.

[9] K. Fujikawa and A. Yamada, Phys. Rev. D **49** (1994) 5890; K. S. Babu, K. Fujikawa and A. Yamada, Phys. Lett. B **333** (1994) 196 [arXiv:hep-ph/9312315]; P. L. Cho and M. Misiak, Phys. Rev. D **49** (1994) 5894 [arXiv:hep-ph/9310332]. For a review of B physics in LR models, see M. Gronau, B Decays, second edition, ed. S. Stone, World Scientific, 1994, p. 644.

[10] T. Mannel and S. Recksiegel, Acta Phys. Polon. B **28** (1997) 2489 [arXiv:hep-ph/9710287].

[11] G. Hiller and A. Kagan, Phys. Rev. D **65** (2002) 074038 [arXiv:hep-ph/0108074].

[12] F. Legger and T. Schietinger, Phys. Lett. B **645** (2007) 204 [Erratum-ibid. B **647** (2007) 527] [arXiv:hep-ph/0605245].

[13] M. Gronau and D. Pirjol, Phys. Rev. D **66** (2002) 054008 [arXiv:hep-ph/0205065].

[14] D. Atwood, T. Gershon, M. Hazumi and A. Soni, arXiv:hep-ph/0701021.

[15] V. D. Orlovsky and V. I. Shevchenko, arXiv:0708.4302 [hep-ph].

[16] D. Atwood, T. Gershon, M. Hazumi and A. Soni, Phys. Rev. D **71** (2005) 076003 [arXiv:hep-ph/0410036].

[17] W. Verkerke and D. Kirkby, *In the Proceedings of 2003 Conference for Computing in High-Energy and Nuclear Physics (CHEP 03), La Jolla, California, 24-28 Mar 2003, pp MOLT007* [arXiv:physics/0306116].

[18] L. Shchutska, A. Golutvin and I. Belyaev, "Study of radiative penguin decays $\mathrm{B}^0 \to \mathrm{K}^{*0}\gamma$ and $\mathrm{B_s} \to \phi\gamma$ at LHCb", CERN-LHCb-2007-030

[19] W. M. Yao *et al.* [Particle Data Group], J. Phys. G **33** (2006) 1.

[20] A. Abulencia *et al.* [CDF Collaboration], Phys. Rev. Lett. **97** (2006) 242003 [arXiv:hep-ex/0609040].

[21] M. Calvi, O. Leroy and M. Musy, "Flavour tagging algorithms and performances in LHCb", CERN-LHCb-2007-058.

[22] J. Borel, L. Nicolas, O. Schneider and J. van Hunen, "The $B_s \to D_s^- \pi^+$ and $B_s \to D_s^\mp K^\pm$ selections", CERN-LHCb-2007-017; S. Cohen, E. Rodrigues and M. Merk, "$\gamma + \phi_s$ sensitivity studies from combined $B_s^0 \to D_s^- \pi^+$ and $B_s^0 \to D_s^\mp K^\pm$ samples at LHCb", CERN-LHCb-2007-041.

[23] L. Fernández, "The sensitivity to the $B_s - \bar{B}_s$ mixing phase at LHCb", CERN-LHCb-2006-047.